

IR and UV Galaxies at $z=0.6$ — Evolution of Dust Attenuation and Stellar Mass as Revealed by SWIRE and GALEX

C. Kevin Xu^{1,5}, David Shupe⁶, Veronique Buat⁹, Michael Rowan-Robinson³, Thomas Babbedge³, Jorge Iglesias-Páramo¹⁰, Tsutomu T. Takeuchi¹¹, Tom A. Barlow¹, Tim Conrow¹, Fan Fang⁶, Karl Forster¹, Peter G. Friedman¹, Eduardo Gonzales-Solares⁸, Carol Lonsdale⁵, D. Christopher Martin¹, Patrick Morrissey¹, Susan G. Neff⁴, David Schiminovich¹, Mark Seibert¹, Todd Small¹, Gene Smith⁷, Jason Surace⁶, Ted K. Wyder¹

ABSTRACT

We study dust attenuation and stellar mass of $z \sim 0.6$ star-forming galaxies using new SWIRE observations in IR and GALEX observations in UV. Two samples are selected from the SWIRE and GALEX source catalogs in the SWIRE/GALEX field ELAIS-N1-00 ($\Omega = 0.8 \text{ deg}^2$). The UV selected sample has 600 galaxies with photometric redshift (hereafter photo- z) $0.5 \leq z \leq 0.7$ and $\text{NUV} \leq 23.5$ (corresponding to $L_{\text{FUV}} \geq 10^{9.6} L_{\odot}$). The IR selected sample contains 430 galaxies with $f_{24\mu\text{m}} \geq 0.2 \text{ mJy}$ ($L_{\text{dust}} \geq 10^{10.8} L_{\odot}$) in the same photo- z range. It is found that the mean $L_{\text{dust}}/L_{\text{FUV}}$ ratios of the $z=0.6$ UV galaxies are consistent with that of their $z=0$ counterparts of the same L_{FUV} . For IR galaxies,

¹California Institute of Technology, MC 405-47, 1200 East California Boulevard, Pasadena, CA 91125

²Laboratoire d'Astrophysique de Marseille, BP 8, Traverse du Siphon, 13376 Marseille Cedex 12, France

³Astrophysics Group, Blackett Laboratory, Imperial College of Science Technology and Medicine, Prince Consort Road, London SW7 2BZ, UK

⁴Laboratory for Astronomy and Solar Physics, NASA Goddard Space Flight Center, Greenbelt, MD 20771

⁵Infrared Processing and Analysis Center, California Institute of Technology 100-22, Pasadena, CA 91125

⁶Spitzer Science Center, California Institute of Technology, Mail Stop 220-6, Pasadena, CA 91125

⁷Center for Astrophysics and Space Sciences, University of California, San Diego, La Jolla, CA 92093-0424

⁸Institute of Astronomy, Madingley Road, Cambridge CB3 0HA, UK

⁹ Observatoire Astronomique Marseille Provence, Laboratoire d'Astrophysique de Marseille, 13012 Marseille, France

¹⁰ Instituto de Astrofísica de Andalucía (CSIC), Camino Bajo de Hueter 50, 18008 Granada, Spain

¹¹ Astronomical Institute, Tohoku University, Aoba, Aramaki, Aoba-ku, Sendai 980-8578, Japan

the mean $L_{\text{dust}}/L_{\text{FUV}}$ ratios of the $z=0.6$ LIRGs ($L_{\text{dust}} \sim 10^{11} L_{\odot}$) are about a factor of 2 lower than local LIRGs, whereas $z=0.6$ ULIRGs ($L_{\text{dust}} \sim 10^{12} L_{\odot}$) have the same mean $L_{\text{dust}}/L_{\text{FUV}}$ ratios as their local counterparts. This is consistent with the hypothesis that the dominant component of LIRG population has changed from large, gas rich spirals at $z > 0.5$ to major-mergers at $z=0$. The stellar mass of $z=0.6$ UV galaxies of $L_{\text{FUV}} \leq 10^{10.2} L_{\odot}$ is about a factor 2 less than their local counterparts of the same luminosity, indicating growth of these galaxies. The mass of $z=0.6$ UV luminous galaxies (UVLGs: $L_{\text{FUV}} > 10^{10.2} L_{\odot}$) and IR selected galaxies, which are nearly exclusively LIRGs and ULIRGs, is the same as their local counterparts.

Subject headings: dust: extinction – galaxies: active – galaxies: evolution – infrared: galaxies – ultraviolet: galaxies

1. Introduction

The early results from rest-frame UV surveys (Lilly et al. 1996; Madau et al. 1996) reveals an order of magnitude higher star formation rate in $z \sim 1$ galaxies compared to local galaxies. This has been confirmed by recent large scale UV surveys carried out by Galaxy Evolution Explorer (hereafter GALEX, Martin et al. 2005). The UV luminosity functions for GALEX sources at $z \sim 1$ (Arnouts et al 2005; Schiminovich et al. 2005) and GALEX number counts (Xu et al. 2005) are consistent with a luminosity evolution index $\alpha \sim 2.5$ (evolution rate $\propto (1+z)^{\alpha}$). The IR/sub-mm surveys reveal a slightly stronger evolution for IR galaxies in the same redshift range, which is also predominantly luminosity evolution with an evolution index in the range of $3 \lesssim \alpha \lesssim 4$ (Blain et al. 1999; Xu 2000; Chary & Elbaz 2001; Le Floch 2005; Babbedge et al. 2006). In an SDSS study of star formation history of local galaxies (‘fossil analysis’), Heavens et al. (2004) concluded that the peak of star formation of the universe is at $z \sim 0.7$. Comparing the luminosity density in the UV (Schiminovich et al. 2005) and that in the FIR (Le Floch et al. 2005) at different redshifts, the ratio $\rho(FIR)/\rho(FUV)$ increases by about a factor of 4 from $z=0$ to $z=1$, indicating a significant evolution in the dust attenuation in star forming galaxies during this epoch (Takeuchi et al. 2005b).

The most significant obstacle preventing accurate measurements of star formation related quantities is the dust attenuation. The best way to constrain the dust attenuation is through the comparison between the UV and infrared emissions (Xu & Buat 1995; Wang & Heckman 1996; Meurer et al. 1999; Gordon 2000). For local galaxies, the UV/IR comparison has been widely carried out using vacuum UV (100 – 2000Å) data and IRAS observations

(Buat & Xu 1996; Wang & Heckman 1996; Heckman et al. 1998; Iglesias-Páramo et al. 2004). Recent studies using new UV observations obtained in the GALEX survey (Martin et al. 2005; Buat et al. 2005; Iglesias-Páramo et al. 2006; Xu et al. 2006) lead to more accurate estimates for the dust attenuation and its dependence on the star formation rate, and the selection effects in the UV and IR samples. There has been limited analysis of the UV/IR comparison of $z > 0.4$ galaxies using ISO data and rest-frame near-UV (2800Å) observations (Flores 1998; Hammer et al. 2005), indicating much higher dust attenuation in these galaxies than that derived from UV-optical SED fits (Hammer et al. 2005). Studies of Spitzer observations of COMBO-17 galaxies found no evidence for evolution of the IR-to-UV ratio versus the star formation rate (SFR) relation over the last 7 Gyrs (Bell et al. 2005; Zheng et al. 2006)

In this paper, we report a study on UV/IR comparisons for galaxies of photometric redshifts $0.5 \leq z \leq 0.7$. Two samples, one UV selected and the other IR selected, are investigated. Galaxies in both samples are star forming galaxies, with the UV sample including favorably the galaxies with low dust attenuation and the IR sample the galaxies with high dust attenuation (Xu et al. 2006; Buat et al. 2006). We use UV data from the GALEX survey and IR data from the Spitzer Wide-area Infrared Extragalactic (SWIRE) survey (Lonsdale et al. 2004) to derive the dust attenuation and stellar mass of these galaxies. Comparisons with their local counterparts constrain the evolution of these properties in the UV and IR selected galaxies, respectively. In order to take into account the effects due to different selection functions for the $z=0.6$ samples and $z=0$ control samples, the comparisons are carried out in luminosity bins where galaxies are found in both the $z=0.6$ and $z=0$ samples.

There is a technical consideration for selecting galaxies at $z \sim 0.6$, in addition to the fact that this redshift is close to the peak of cosmic star formation rate found by Heavens et al. (2004): At $z \sim 0.6$, the GALEX NUV band (2350Å) measures the rest-frame FUV band (1530Å), Spitzer IRAC $3.6\mu m$ band is close to rest-frame K band ($2.2\mu m$), and the MIPS $24\mu m$ band is close to the rest-frame $15\mu m$. The rest-frame K band luminosity is the best indicator of stellar mass (Bell et al. 2003), and the rest-frame $15\mu m$ luminosity as an indicator of integrated IR luminosity ($5 - 1000\mu m$) has been thoroughly investigated in the context of ISOCAM $15\mu m$ observations (Flores et al. 1999; Franceschini et al. 2001; Chary & Elbaz et al. 2001). Therefore comparisons between $z=0.6$ galaxies and $z=0$ galaxies in the corresponding bands will suffer minimum errors due to the k-corrections which can be rather uncertain in the far-UV and MIR wavebands.

The paper is organized as following: After this introduction, the data sets analyzed in this paper are presented in Section 2. Major results are listed in Section 3. Systematic

uncertainties are discussed in Section 4. Section 5 and Section 6 are devoted to the discussion and conclusion, respectively. Through out this paper, we assume $\Omega_\Lambda = 0.7$, $\Omega_m = 0.3$, and $H_0 = 70 \text{ km sec}^{-1} \text{ Mpc}^{-1}$.

2. Data and Sample Selection

2.1. GALEX and SWIRE data

The data investigated are in the GALEX field ELAIS-N1-00, a circular area of 1 deg diameter centered at RA= $16^{\text{h}}13^{\text{m}}36^{\text{s}}.8$ and Dec= $54^\circ59'03''.3$, corresponding to a sky coverage of 0.8 deg^2 . The field has been observed by both GALEX and SWIRE surveys. The SWIRE $3.6\mu\text{m}$ and $24\mu\text{m}$ images and fluxes are taken from “The SWIRE N1 Image Atlases and Source Catalogs” (Surace et al. 2004). The nominal 5σ sensitivity limit of the SWIRE $24\mu\text{m}$ survey is $f_{24} = 0.2 \text{ mJy}$, but below $f_{24} = 0.25 \text{ mJy}$ the catalog becomes progressively incomplete (Surace et al. 2004; Shupe et al. 2006). The GALEX NUV (2350\AA) image, a coadd of observations of 8 orbits with a total $T_{exp}=7899 \text{ sec}$, is taken from GALEX first public data release (GALEX-DR1). NUV sources are extracted from the GALEX image using IRAF DAOPHOT task. An average foreground extinction of $A_{NUV} = 0.07 \text{ mag}$, estimated using Schlegel map (Schlegel et al. 1998), has been corrected. Detailed inspections show that the $5\text{-}\sigma$ detection reaches NUV= 23.5 mag , which is taken as the flux limit of the NUV catalog. Contaminations due to false sources become more severe at magnitudes fainter than this. IR galaxies and UV galaxies undetected either in the optical r band (down to $r=23.5 \text{ mag}$, Rowan-Robinson et al. 2005) or in the IRAC $3.6\mu\text{m}$ band (with the flux limit $f_{3.6\mu\text{m}} = 3.7\mu\text{Jy}$, Surace et al. 2004) are excluded in this analysis. This significantly reduces the number of false sources in both bands. Some extreme populations such as the ‘extreme $24\mu\text{m}$ galaxies’ (Yan et al. 2005; Houck et al. 2005), will be missed because of the exclusion of sources without optical counterparts. However, these sources are very rare and most of them are hyper-luminous galaxies (HLIRGS) at high redshift ($z \gtrsim 2$; Houck et al. 2005), outside the redshift range of our samples. The selection of sources detected in the IRAC $3.6\mu\text{m}$ band should not introduce any significant bias because observations in this band is more than an order of magnitude deeper than that of the NUV and $f_{24\mu\text{m}}$ surveys for an average SED at $z=0.6$ (see Section 5). Galaxies with the UV and/or the IR emission dominated by the active galactic nuclei (AGN) are not explicitly excluded from this study. It has been shown in the literature that for both the $24\mu\text{m}$ selected samples and the GALEX selected samples, the AGN contamination is insignificant, only about 10 – 15% of sources (Franceschini et al. 2005; Bell et al. 2005; Budavari et al. 2005).

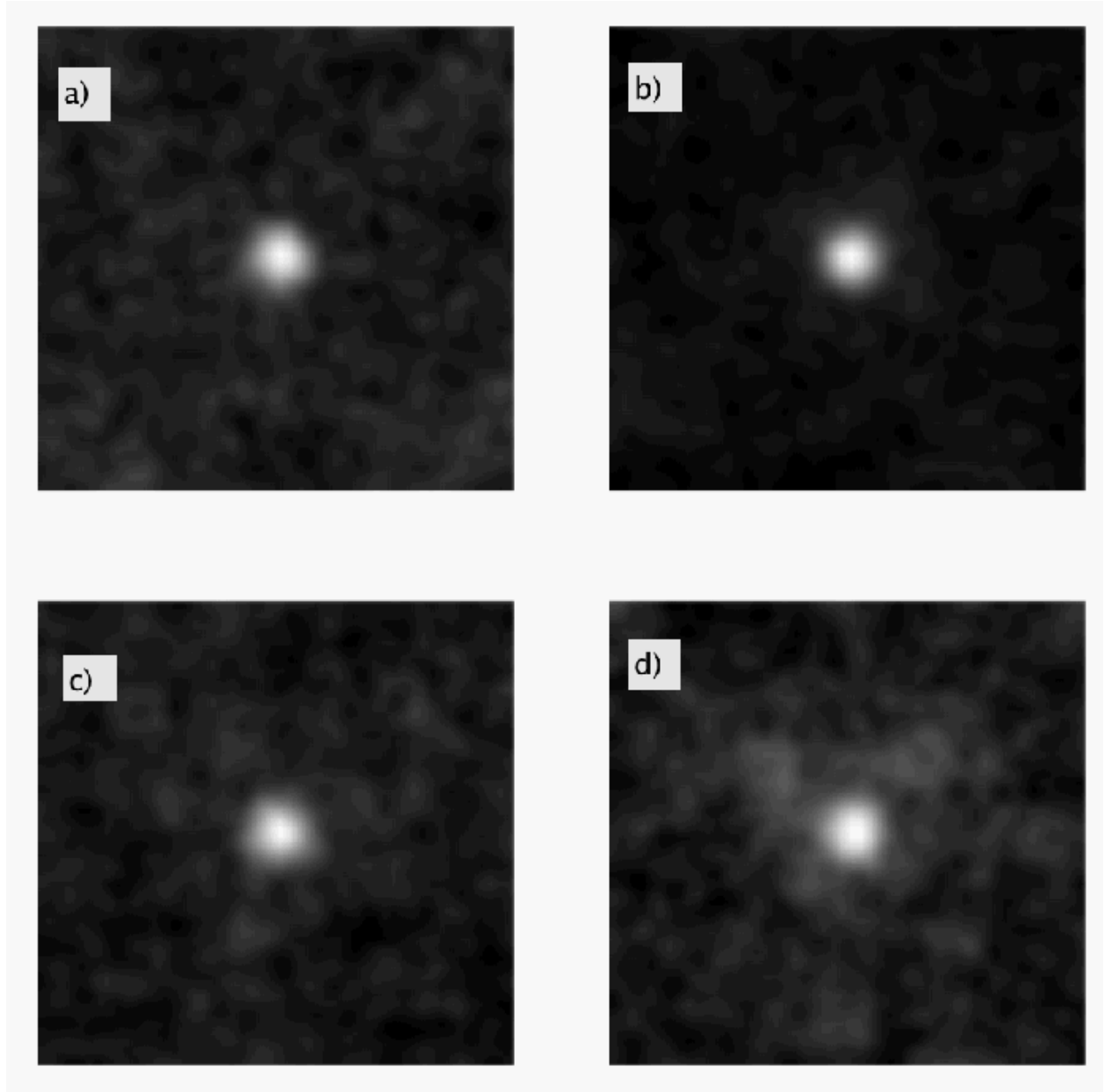


Fig. 1.— Stacked $24\mu m$ images of $z=0.6$ UV sources in the FUV luminosity bins of $9.6 < \log(L_{FUV}/L_{\odot}) \leq 9.9$ (**Panel a**), $9.9 < \log(L_{FUV}/L_{\odot}) \leq 10.2$ (**Panel b**), $10.2 < \log(L_{FUV}/L_{\odot}) \leq 10.5$ (**Panel c**), and $10.5 < \log(L_{FUV}/L_{\odot}) \leq 10.8$ (**Panel d**).

2.2. Photo-z

The SWIRE photometric redshifts (hereafter photo-z) are derived using the template-fitting code IMPZ (Babbedge et al. 2004; Rowan-Robinson 2003). This method considers a set of galaxy and Type 1 AGN templates, along with several priors on dust extinction, stellarity and absolute magnitude with redshift in order to obtain optimal results. It has been extended to incorporate IRAC 3.6 and 4.5 μm data in addition to optical photometry, with the assumption that the emission in the two IRAC short wavelength bands is dominated by the stellar radiation (Babbedge et al. 2006; Rowan-Robinson et al. 2005). The same “simple stellar populations” (SSPs) templates used in Babbedge et al. (2004), which cover from the UV to the NIR (to $\sim 5\mu\text{m}$) are used. The inclusion of the IRAC 3.6 and 4.5 μm band data has been shown to improve both the reliability and precision of the photo-z’s (Babbedge et al. 2006; Rowan-Robinson et al. 2005). In particular, the additional NIR data has enabled the rejection of most of the extreme outliers resulting from optical-only results and reduced the dispersion (more details can be found in Section 3.1.2 of Babbedge et al. 2006, and in Section 5 of Rowan-Robinson et al. 2005). Comparisons to spectroscopic redshifts in ELAIS N1 (Pérez-Fournon et al. 2006; Serjeant et al. 2006; Hatziminaoglou et al. 2005) give a total *rms* scatter, σ_{tot} , of 0.057 for $(1+z)$. This is consistent with Rowan-Robinson et al (2005) who quoted an *rms* of 6.9% of $(1+z)$ for ELAIS-N1, where the majority of sources out to redshift $z\sim 0.5$ are galaxies whilst at higher redshifts (to $z\sim 3$) Type 1 AGN dominate. The success of the code has also been demonstrated for a number of other fields, filter sets and spectroscopic samples (Babbedge et al. 2006). For all the samples, the mean systematic offset between the photometric and spectroscopic redshifts was found to be essentially zero to the precision of the photometric redshifts. For example, the ELAIS-N1 sample has $\overline{\Delta z}/(1+z) = 0.0037$.

It should be noted that photometric redshift fitting requires the photometry in each band being measured in the same way. When only using optical data, use of fixed aperture fluxes is sufficient. However, if we include IRAC NIR (3.6 and 4.5 μm) fluxes it is important to be comparing like with like, and these fluxes are integrated fluxes. Hence, for the optical bands, the aperture magnitudes corrected to the integrated magnitudes via curve-of-growth analysis are used. This procedure could introduce errors for galaxies whose integrated SEDs differ largely from the SEDs of their central regions, but in practice the results are consistent, as found in Babbedge et al. (2006).

Another issue is on the potential mis-identifications between optical sources and IRAC sources due to source confusion, which in turn might affect the accuracy of the photo-z results. The accuracy of the cross-IDs of IRAC and optical catalogs of SWIRE sources has been discussed extensively in Surace et al. (2004). The flux limits of both the IRAC and optical catalogs are well above the confusion limits (Fazio et al. 2004, Surace et al., private com-

munication), therefore the probability of mis-identification due to chance confusion in either band is much less than 1%. Furthermore, the angular resolution of the optical (FWHM $\sim 1'' - 1''.5$) and that of the IRAC 3.6 and 4.5 μm bands (FWHM $\sim 1''.6$) are not very different from each other. Hence, even the genuine close sources (such as galaxy mergers) tend to have the same status as being resolved or confused in both the optical and the IRAC bands in the same time. The effect of the confusion on the photo-z results should be insignificant.

2.3. Samples

The **UV sample**, selected in the area considered here and in the photo-z range of $0.5 \leq z \leq 0.7$, has 600 NUV sources brighter than NUV=23.5 mag. Among them, 117 are detected by Spitzer at $24\mu\text{m}$ with $f_{24} \geq 0.2$ mJy, corresponding to an IR detection rate of 20%. For GALEX sources undetected at $24\mu\text{m}$, upperlimits of $f_{24} = 0.2$ mJy are assigned.

The **IR sample** contains 430 SWIRE sources of $f_{24} \geq 0.2$ mJy, selected in the same area and the same photo-z range ($0.5 \leq z \leq 0.7$). Their detection rate by GALEX in NUV is 27%. NUV flux upperlimits corresponding to NUV=23.5 mag are assigned to those sources undetected by GALEX.

For both UV and IR samples, rest-frame FUV luminosities ($\nu L_\nu(1530\text{\AA})$) are derived from the NUV (2350 \AA) magnitudes and the photo-z. The Spitzer $24\mu\text{m}$ observations measure the rest-frame $15\mu\text{m}$ emission in these $z \sim 0.6$ galaxies, and the total dust luminosity is estimated using the conversion factor $L_{dust} = 11.1 \times L_{15}$ (Chary & Elbaz 2001).

The rest-frame K band ($2.2\mu\text{m}$) luminosity is calculated using $f_{3.6}$ and the photo-z. Stellar mass is estimated from the K-band luminosity using the mass-to-light ratio $M_{\text{stars}}/L_K = 0.6M_\odot/L_\odot$ (Bell et al. 2003), based on a Kroupa IMF (Kroupa et al. 1993). This is about a factor of 2 lower than the mass-to-light ratio derived using Salpeter IMF (Cole et al. 2001).

Because we are investigating galaxies at a given redshift, the magnitude limit (NUV=23.5 mag) of the UV selected sample corresponds to a UV luminosity limit of $L_{FUV} = 10^{9.6} L_\odot$ (assuming $z=0.6$), and the flux limit of the $24\mu\text{m}$ selected sample corresponds to an IR luminosity limit of $L_{dust} = 10^{10.8} L_\odot$. Therefore, we are only looking at galaxies in the bright part of the UV and IR luminosity functions. Particularly, for the IR selected sample, we study nearly exclusively LIRGs ($L_{dust} \geq 10^{11} L_\odot$) and ULIRGs ($L_{dust} \geq 10^{12} L_\odot$). Given the close to zero mean systematic offset between the photometric and spectroscopic redshifts, our statistical results should be robust against occasional large errors of the photo-z for some individual galaxies ('outliers').

The **control samples** at $z=0$ are taken from Xu et al. (2006), which are similar to those used in Buat et al. (2005), Iglesias-Páramo et al. (2006). The UV sample at $z=0$ includes 94 galaxies brighter than $NUV = 16$ mag selected from GALEX G1 stage All-sky Imaging Survey (AIS), covering 654 deg^2 . The $z=0$ FIR sample includes 161 galaxies with $f_{60} \geq 0.6 \text{ Jy}$ in 509 deg^2 sky covered both by GALEX AIS and IRAS PSCz (Saunders et al. 2000). More details can be found in Xu et al. (2006), Buat et al (2005) and Iglesias-Páramo et al. (2006). Since many quantities (such as the dust attenuation) have strong luminosity dependence, we always compare the $z=0.6$ and $z=0$ galaxies in the same luminosity bins.

3. Results

3.1. Dust Attenuation in $z=0.6$ Galaxies

3.1.1. UV Galaxies at $z=0.6$

The $24\mu\text{m}$ detection rate of the $z=0.6$ NUV sources is only 20% (Section 2). Therefore for a large majority of these sources the MIR emission is below the SWIRE sensitivity limit. In order to derive meaningful statistics related to the infrared emission, we carried out stacking analysis for galaxies binned into four UV luminosity bins (Table 1).

For each NUV galaxy included in a bin, we cut from the background-subtracted $24 \mu\text{m}$ mosaic a small subimage, 1 arcminute on a side, and centered on the coordinates given in the GALEX catalog. From a stack of these subimages, we compute a trimmed mean image, excluding 20% of the subimages with the lowest and highest brightness (10% at either end). The purpose of the trimming is to guard against contamination from nearby bright sources, as well as mis-classified sources with large photo- z errors (‘outliers’). The mean flux density is measured from the trimmed mean image in an aperture of $18''$ diameter. To estimate the standard error of the mean flux density, we use a bootstrap method. From the stack of subimages, we sample with replacement the subimages and make a new trimmed mean image, and measure the flux density in the aperture. The resampling is repeated 1000 times, and the sample standard deviation of the aperture measurements provides the uncertainty estimate. The average $\log(L_{\text{dust}}/L_{\text{FUV}})$ is derived from the mean f_{24} , mean redshift $z=0.6$, and the mean L_{dust} of the bin. The error of mean $\log(L_{\text{dust}}/L_{\text{FUV}})$ is the quadratic sum of the error of f_{NUV} and that of $\langle L_{\text{dust}} \rangle$. The stacked (trimmed mean) images are shown in Fig.1. The results are reported in Table 1.

In Fig.2 we compare the $L_{\text{dust}}/L_{\text{FUV}}$ ratios of the $z=0.6$ UV galaxies with those of the $z=0$ UV galaxies in the control sample. The FUV attenuation (A_{FUV}) values corresponding

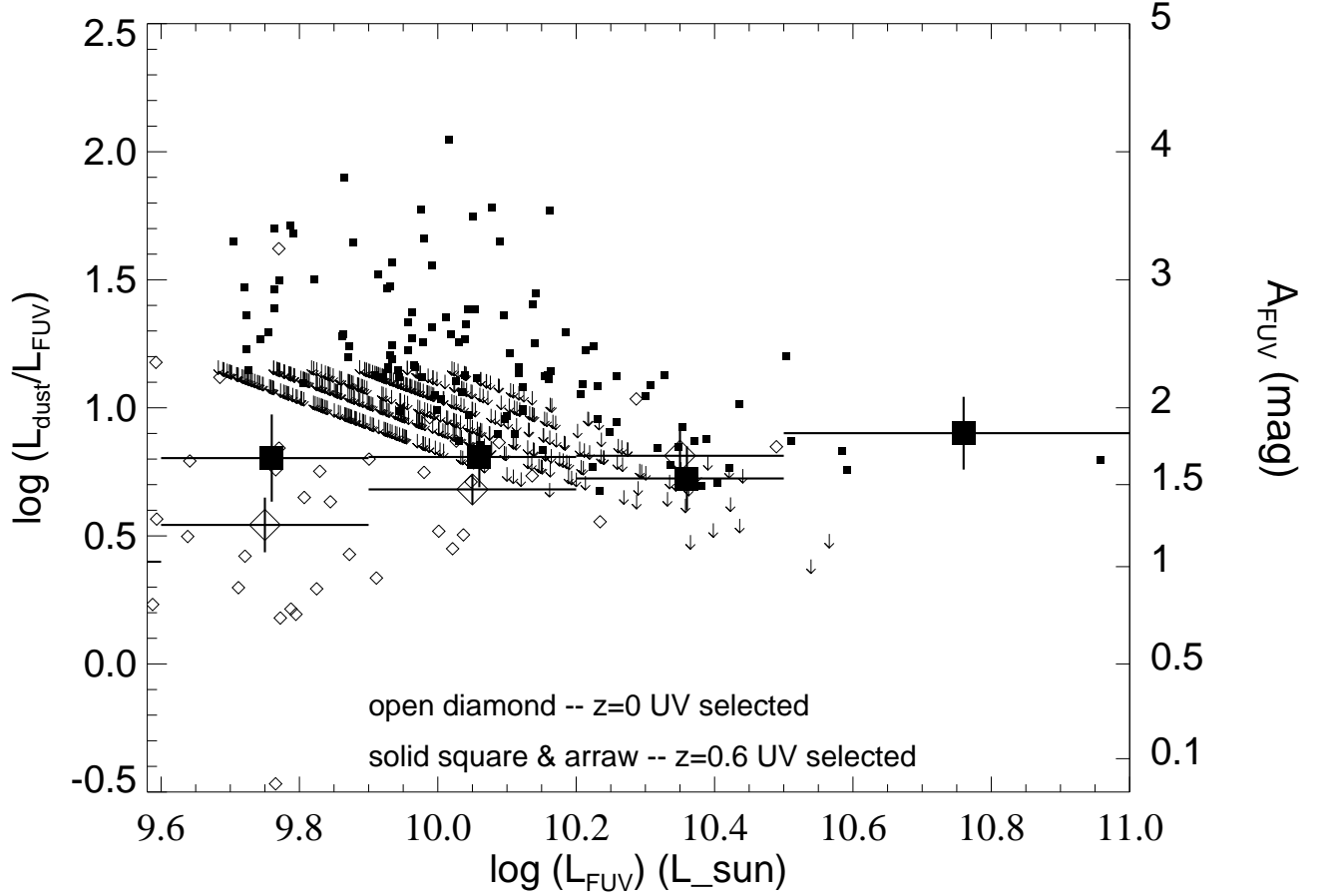


Fig. 2.— $\log(L_{\text{dust}}/L_{FUV})$ v.s. $\log(L_{FUV})$ plot for the UV selected samples at $z=0.6$ and $z=0$. Arrows denote upperlimits. Large solid squares with error bars are the means for $z=0.6$ galaxies, derived through stacking analysis. Large open diamonds with error bars are the means for $z=0$ galaxies. The right hand axis of the plot marks the FUV attenuation (A_{FUV}) corresponding to the $\log(L_{\text{dust}}/L_{FUV})$.

to given $\log(L_{dust}/L_{FUV})$, marked on the right hand axis of the plot, are calculated using the following formula taken from Buat et al. (2005):

$$A_{FUV} = -0.00333y^3 + 0.3522y^2 + 1.1960y + 0.4967, \quad (1)$$

where $y = \log(L_{dust}/L_{FUV})$. Small solid squares and arrows represent individual $z=0.6$ galaxies, and small open diamonds the $z=0$ galaxies. The arrows, denoting the upper-limits in the $z=0.6$ sample, concentrate in a narrow, tilted region. This is because the redshifts (photo- z) of the galaxies in this sample are in a very narrow range of $0.5 \leq z \leq 0.7$. Therefore the $25\mu m$ upper limits (0.2 mJy) are translated to a narrow range of L_{dust} upper limits. The large symbols with error bars are the mean ratios in the corresponding luminosity bins. For the $z=0.6$ sample, they are calculated from the average $25\mu m$ fluxes measured on the stacked images. As demonstrated in Fig.1, good detections are obtained in all four stacked $24\mu m$ images. Therefore, unlike for ratios of individual galaxies, the mean L_{dust}/L_{FUV} ratios are not affected by sensitivity limit of the SWIRE survey. For the $z=0$ sample, since all individual sources are detected in the IR band, the calculations of the means are straightforward.

For both $z=0.6$ and $z=0$ samples, the L_{dust}/L_{FUV} ratio does not show significant dependence on the UV luminosity. It is interesting to note that many $z=0.6$ UV galaxies with $\log(L_{FUV}) < 10.2$ have $\log(L_{dust}/L_{FUV}) > 1.5$, corresponding to the FUV attenuation $A_{FUV} \gtrsim 3$ mag (Buat et al. 2005), whereas such high dust attenuation is seldomly seen in their local counterparts. In the UV luminosity bin of $9.6 \leq \log(L_{FUV}/L_{\odot}) < 9.9$, the mean L_{dust}/L_{FUV} ratios of $z=0$ and $z=0.6$ galaxies show a $\sim 80\%$ (i.e. 0.25 dex) difference at $\sim 1\sigma$ level. In the remaining two luminosity bins where the two samples overlap, the mean L_{dust}/L_{FUV} ratios of $z=0$ and $z=0.6$ galaxies are very close to each other (difference $< 50\%$). Recently, Burgarella et al. (2006) found evidence for about half of $z \sim 1$ UV bright galaxies to have very low dust attenuation ($A_{FUV} \sim 0.5 - 0.6$ mag). We did not detect the same trend for $z \sim 0.6$ UV galaxies.

Table 1. Mean IR fluxes and IR-to-UV ratios of $z=0.6$ UV galaxies.

| $\log L_{FUV}$ (L_{\odot}) | N_{tot} | N_{det} | f_{24}^{stack} (μJy) | σ (μJy) | $\log(L_{dust}/L_{FUV})$ | error |
|-----------------------------------|-----------|-----------|----------------------------------|--------------------------|--------------------------|-------|
| 9.75 ± 0.15 | 187 | 21 | 67 | 25 | 0.80 | 0.17 |
| 10.05 ± 0.15 | 341 | 68 | 135 | 21 | 0.80 | 0.12 |
| 10.35 ± 0.15 | 65 | 24 | 222 | 42 | 0.72 | 0.13 |
| 10.65 ± 0.15 | 7 | 5 | 838 | 219 | 0.90 | 0.14 |

3.1.2. IR Galaxies at $z=0.6$

For the 430 $z=0.6$ galaxies in the $24\mu\text{m}$ selected sample, the detection rate in the GALEX NUV band is also low (27%). Therefore the stacking analysis is again exploited in deriving the mean NUV fluxes. Galaxies are binned into four IR luminosity bins (Table 2). Because the depth of the NUV image is very close to the confusion limit (NUV=24 mag, Xu et al. 2005), we choose to subtract sources brighter than NUV=23.5 mag (5σ detections) from the image before stacking. In principle this approach should yield a cleaner result (Zheng et al. 2006) than simply stacking all sources because the contamination due to bright neighboring sources outside the sample (i.e. sources of different redshifts) is minimized. Again, we derive the trimmed mean of the NUV flux for each bin of IR selected galaxies by excluding 20% of galaxies with the highest and the lowest measured NUV fluxes (10% on each side), and estimate the errors by bootstrapping (1000 replicate simulations). For each L_{dust} bin, the average $\log L_{dust}/L_{FUV}$ and its error are derived in the same way as for UV galaxies in a given L_{FUV} bin. The results are reported in Table 2.

In Fig.3 we compare the L_{dust}/L_{FUV} ratios of the $z=0.6$ IR galaxies with those of their $z=0$ counterparts. Same as in Fig.2, small symbols and arrows represent individual galaxies, and large symbols with error bars the means in corresponding luminosity bins. In contrast with the UV galaxies in Fig.2, both $z=0.6$ and $z=0$ IR galaxies show strong dependence of the L_{dust}/L_{FUV} ratio with the luminosity. In the luminosity range covered by the $z = 0.6$ sample ($\gtrsim 10^{11} L_{\odot}$), the L_{dust}/L_{FUV} ratios of IR galaxies are one to two orders of magnitude higher than those of the UV galaxies (Fig.2). It appears that $z=0.6$ IR galaxies have a steeper slope in the $\log(L_{dust}/L_{FUV})$ versus $\log(L_{dust})$ relation than $z=0$ IR galaxies. The mean L_{dust}/L_{FUV} of $z=0.6$ galaxies in the bin $10.8 \leq \log(L_{dust}/L_{\odot}) < 11.2$ is significantly lower, by a factor of ~ 2.5 , than that of their local counterparts, indicating that $z=0.6$ LIRGs ($\log(L_{dust}/L_{\odot}) \sim 11$) have lower dust attenuation compared to their local counterparts. On

Table 2. Mean UV fluxes and IR-to-UV ratios of $z=0.6$ IR galaxies.

| $\log(L_{dust})$ (L_{\odot}) | N_{tot} | N_{det} | NUV^{stack} (mag) | σ (mag) | $\log(L_{dust}/L_{FUV})$ | error |
|-------------------------------------|-----------|-----------|------------------------|-------------------|--------------------------|-------|
| 11.0 ± 0.2 | 172 | 52 | 24.15 | 0.20 | 1.37 | 0.11 |
| 11.35 ± 0.15 | 200 | 50 | 24.30 | 0.18 | 1.74 | 0.11 |
| 11.65 ± 0.15 | 49 | 12 | 24.22 | 0.28 | 2.04 | 0.12 |
| 12.0 ± 0.2 | 9 | 3 | 23.76 | 0.39 | 2.25 | 0.16 |

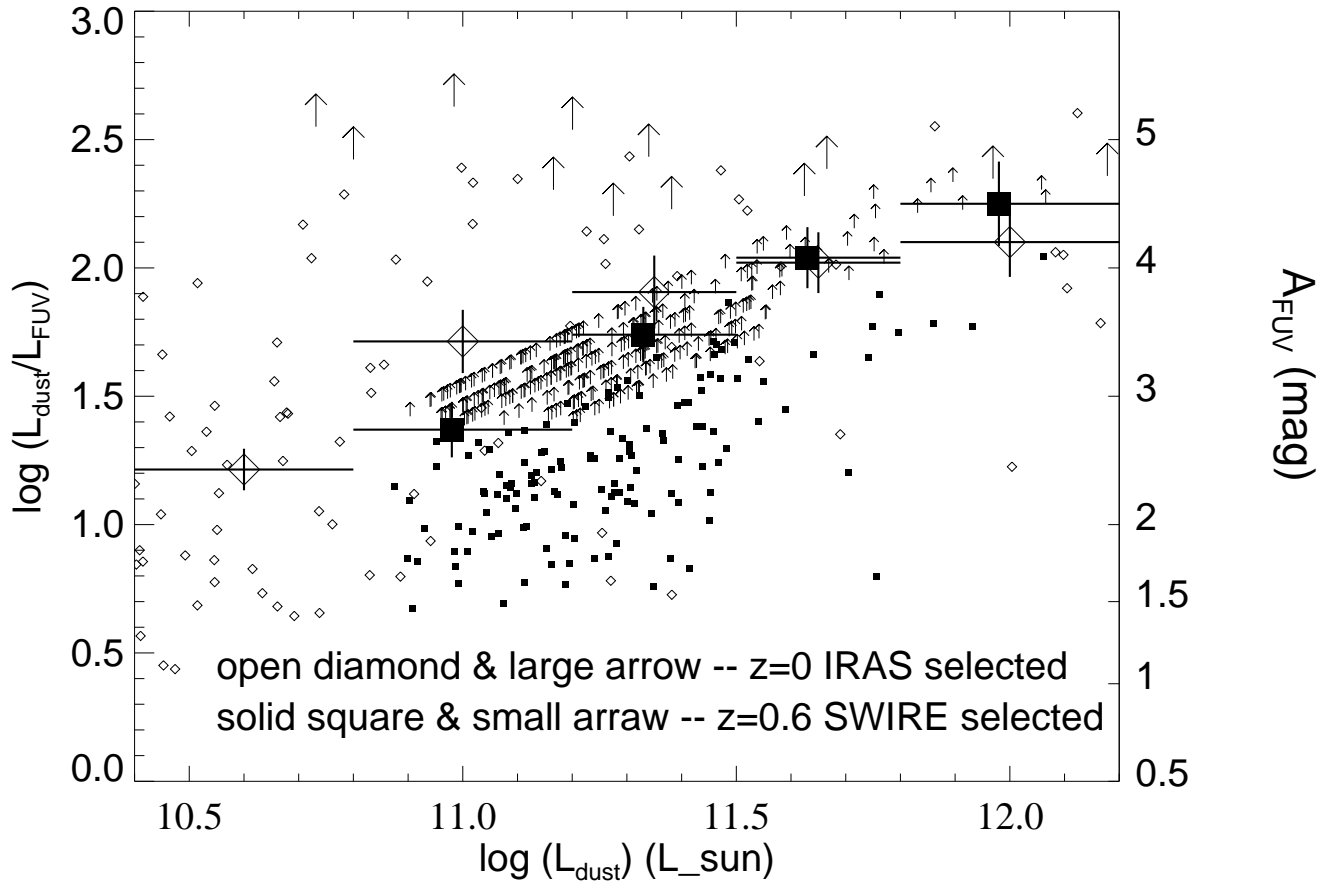


Fig. 3.— L_{dust}/L_{FUV} v.s. L_{dust} plot for the IR selected samples at $z=0.6$ and $z=0$. Arrows denote upperlimits. The large solid squares with error bars are the means for $z=0.6$ galaxies. The large open diamonds with error bars are the means for $z=0$ galaxies.

the other hand, as shown in Fig.3, $z=0.6$ ULIRGs ($\log(L_{\text{dust}}/L_{\odot}) \sim 12$) have similar dust attenuation as local ULIRGs.

Bell et al. (2005) and Zheng et al. (2006), in their studies of MIPS observations of COMBO-17 galaxies, concluded that there is no evolution in the $L_{\text{dust}}/L_{\text{FUV}}$ versus SFR relation over the last 7 Gyr. It is not straightforward to compare their results with ours because our sample is IR selected whereas COMBO-17 is an optical sample. The analysis of Bell et al. (2005) is based on a comparison of the $L_{\text{dust}}/L_{\text{FUV}}$ versus SFR plot of individual $z \sim 0.7$ galaxies with that of their local counterparts (Fig.1 of Bell et al. 2005), which can be affected by the presence of large fraction ($\sim 70\%$) of upperlimits in the MIPS data. In Fig.9 of Zheng et al. (2006), only galaxies in the top two panels (corresponding to the M_B bins of $[M_* - 1, M_*]$ and $[M_*, M_* + 1]$) include LIRGs ($\text{SFR} > 10M_{\odot} \text{ yr}^{-1}$). For these galaxies, there is indeed a trend that while the average SFR increases by about an order of magnitude from $z=0.15$ to $z=0.95$, the $L_{\text{dust}}/L_{\text{FUV}}$ ratio increases very little, at least significantly less than what is predicted by the $L_{\text{dust}}/L_{\text{FUV}}$ versus SFR relation. Le Floc'h et al (2005) studied a MIPS selected sample (median redshift ~ 0.7) among COMBO-17 galaxies. Inspections of their $L_{\text{IR}}/L_{\text{UV}}$ versus LIR plot (their Fig.10c) show that the median $L_{\text{IR}}/L_{\text{UV}}$ of the LIRGs in that sample is also significantly lower than that of local LIRGs, consistent with our result.

3.2. Stellar Mass of $z=0.6$ Galaxies

3.2.1. UV Galaxies at $z=0.6$

The stellar mass of $z=0.6$ galaxies is estimated using the IRAC $3.6\mu m$ flux, which measures the rest-frame K-band emission (Section 2.2). For the control samples at $z=0$, the stellar mass is estimated using the total magnitude (m_{tot}) of the 2MASS K_s ($2.16\mu m$) band (Jarrett et al. 2000). Interestingly, as shown in Fig.4, the stellar mass of $z=0.6$ UV galaxies fainter than $L_{\text{FUV}} = 10^{10.2} L_{\odot}$ is on average a factor of 1.5 to 2 lower than that of their local counterparts. This result is statistically significant at the 2σ level. These galaxies are in the category of ‘intermediate massive galaxies’ ($3 \times 10^{10} M_{\odot} \leq M \leq 3 \times 10^{11} M_{\odot}$) as defined by Hammer et al. (2005). According to Heavens et al. (2004), the star formation in these galaxies peaked at $z \sim 0.6$. Hammer et al. (2005) argued that the mass of these galaxies increased by about a factor of 2 since $z=1$. Our result is consistent with this. On the other hand, the $z=0.6$ UV luminous galaxies (UVLGs, Heckman et al. 2005) of $L_{\text{FUV}} > 10^{10.2} L_{\odot}$ have the same mean stellar mass as their local counterparts.

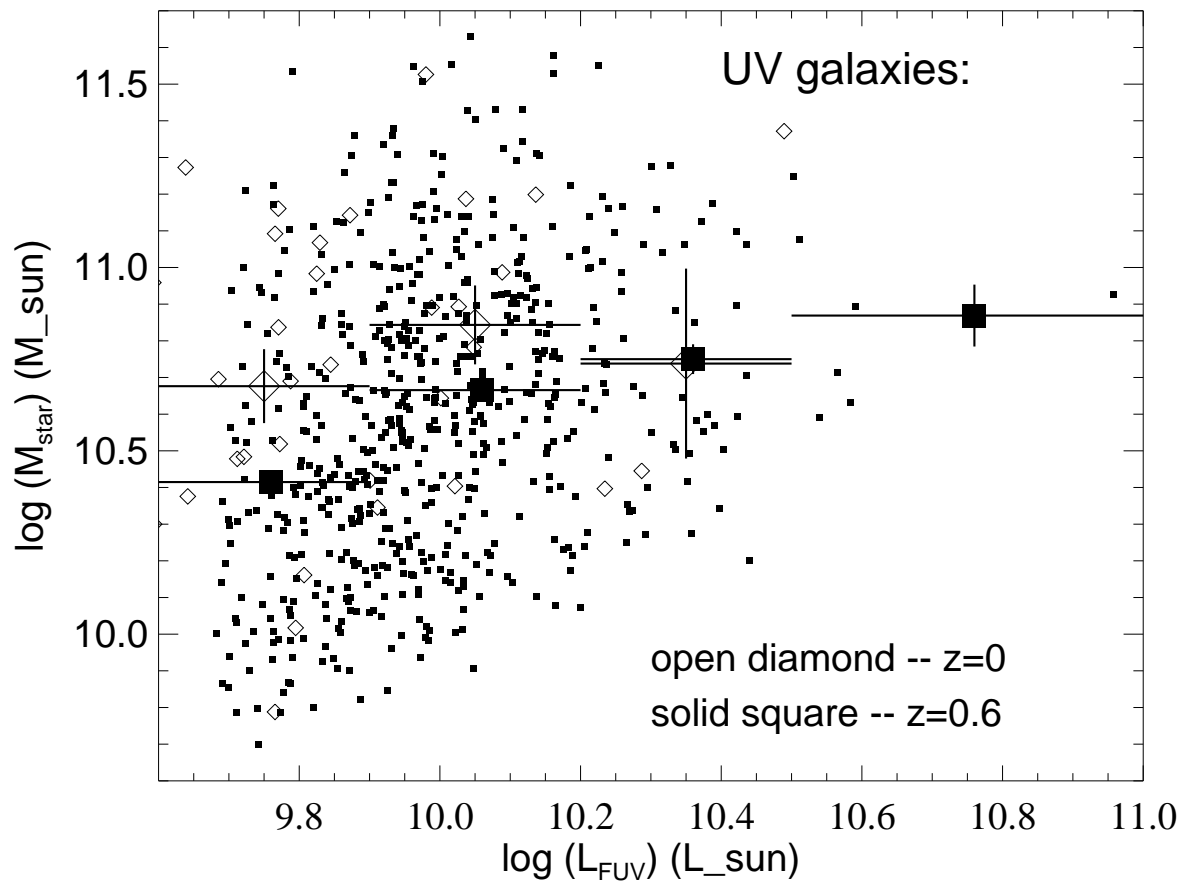


Fig. 4.— Plot of stellar mass (estimated using rest-frame K band luminosity) vs. FUV luminosity for UV selected samples at $z=0.6$ (solid squares) and $z=0$ (open diamonds). The small symbols are individual galaxies, whereas the large symbols with error bars are the corresponding means.

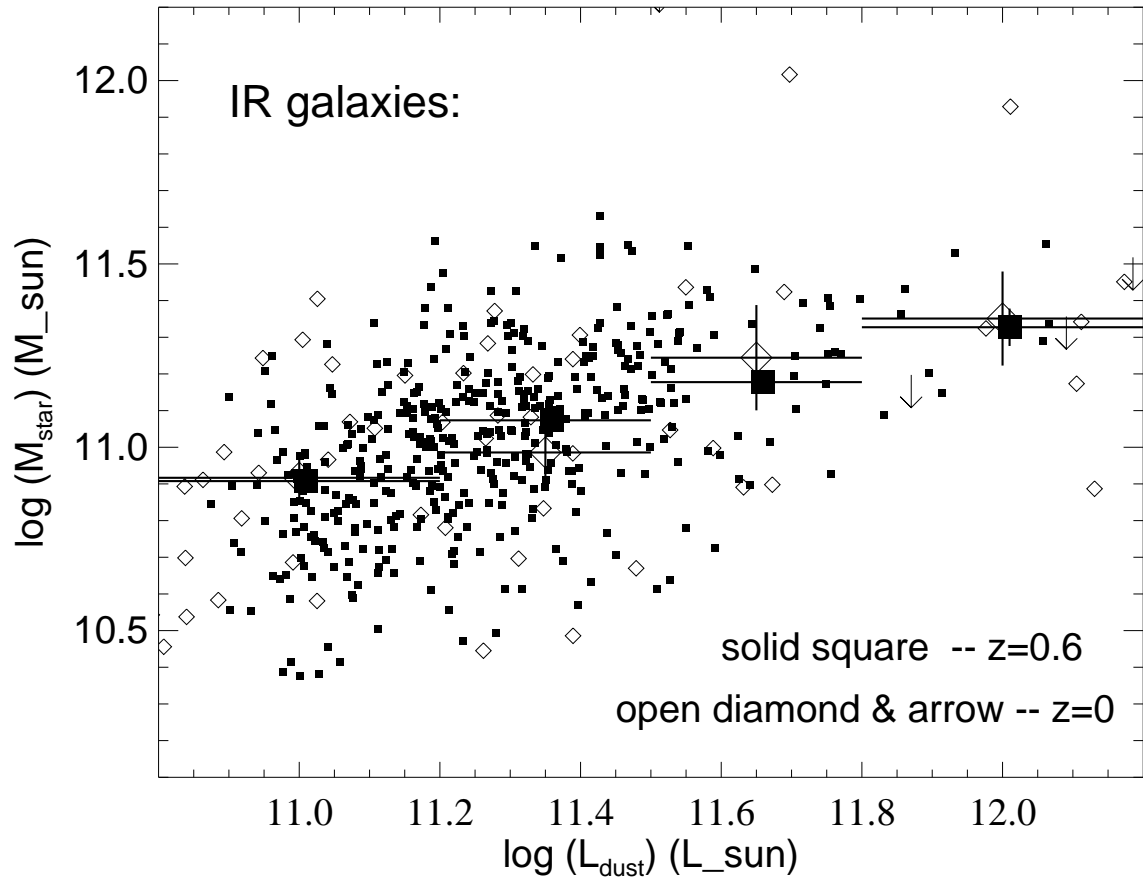


Fig. 5.— Plot of stellar mass vs. L_{dust} for IR selected samples at $z=0.6$ (solid squares) and $z=0$ (open diamonds). The small symbols are individual galaxies, whereas the large symbols with error bars are the corresponding means.

3.2.2. IR Galaxies at $z=0.6$

In Fig.5 we compare the stellar mass of $z=0.6$ IR galaxies with that of their local counterparts. Here, unlike for UV galaxies, no systematic difference is found between the means of $z=0.6$ and $z=0$ galaxies. Both samples show the same trend that more luminous galaxies have higher stellar mass.

It should be pointed out that for bright IR galaxies, particularly the ULIRGs, the contribution from the violent starburst to the rest-frame NIR emission can be significant (Surace et al. 2000), accounting for up to $\sim 50\%$ of the K band flux. Therefore the stellar mass estimated using the rest-frame K-band should be treated with caution. On the other hand, the conclusion derived from Fig.5 should not be affected by this if the contamination from the starburst is the same for the $z=0$ and for the $z=0.6$ galaxies of the same luminosity.

3.2.3. Comparison between UV and IR Galaxies

UV and IR samples select low and high dust attenuation galaxies, respectively (Xu et al. 2006; Buat et al. 2006). Given the dependence of the dust attenuation on stellar mass (Wang & Heckman 1996; Burgarella et al. 2005), the UV galaxies tend to have lower stellar mass than the IR galaxies. This is indeed what we see in Fig.4 and Fig.5. In particular, no IR galaxy in the $z=0.6$ sample has the stellar mass less than $10^{10.3} M_{\odot}$, while as many as about 20% of galaxies in the $z=0.6$ UV sample have stellar mass below this. It should be noted that the IRAC $3.6\mu\text{m}$ band flux limit $f_{3.6\mu\text{m}} = 3.7\mu\text{Jy}$ corresponds to a stellar mass limit of $M = 10^{9.4} M_{\odot}$, a factor of ~ 2 (~ 8) lower than the minimum stellar mass of the $z=0.6$ UV galaxies (IR galaxies). This demonstrates again that very few (if any) galaxies might have been missed by our UV and IR samples due to the IRAC $3.6\mu\text{m}$ flux limit.

UVLGs in the last two UV luminosity bins in Fig.4 have their mean $L_{\text{dust}} > 10^{11} L_{\odot}$ (Table 1), therefore belonging to the LIRG population as well. These are galaxies with the most active star formation in the universe, likely being in the peak phase of some brief (and perhaps recurrent) starburst episodes (Hammer et al. 2005). In the literature, three mechanisms have been considered for the triggering of starbursts, including (1) major-merger, (2) minor merger, (3) bar instability during the secular evolution of disk galaxies (Hammer et al. 2005; Bell et al. 2005; Combes 2006). There is indication that relative importance of these mechanisms has changed since $z \sim 1$ (Melbourne et al. 2005). Our results in Fig.4 and Fig.5 indicate that, no matter which mechanism dominates the triggering of LIRG/ULIRG activity, the host galaxies of these starburst events in the $z=0.6$ and $z=0$ universe have the same stellar mass.

4. Systematic Uncertainties

4.1. The L_{dust}/L_{15} ratio

The most important source of systematic uncertainty in this work is due to the extrapolation from L_{15} to L_{dust} . The analysis of SEDs local IR galaxies by Chary & Elbaz (2001) has shown that $L_{dust} \propto L_{15}^{0.998 \pm 0.021}$, therefore the L_{dust}/L_{15} ratio has little dependence on the luminosity (see also Takeuchi et al. 2005a). We checked this result using the IR SEDs of a larger sample of 831 IRAS galaxies that are constructed ‘semi-empirically’ by Xu et al. (2001). The result is plotted in Fig.6. Xu et al. (2001) divided the SED sample into 3 sub-classes according to the IRAS colors: normal disk galaxies ($f_{60}/f_{25} > 5$ and $f_{100}/f_{60} \geq 2$), starburst galaxies ($f_{60}/f_{25} > 5$ and $f_{100}/f_{60} < 2$), and AGNs ($f_{60}/f_{25} \leq 5$). As shown in Fig.6, indeed for normal disks and starbursts the L_{dust}/L_{15} ratio is rather constant against the luminosity. The mean L_{dust}/L_{15} of normal disk galaxies is 11.5 ± 3.1 and that of starburst galaxies is 11.0 ± 2.8 , both very close to the value of Chary & Elbaz (2001) which is 11.1. On the other hand, there is a significant trend for galaxies with AGN in the sense that the ratio decreases with L_{15} . The mean of IR galaxies with AGN is 4.9 ± 3.8 , about a factor 2 lower than those of normal disk and starburst galaxies. Therefore, we might have significantly over-estimated the L_{dust} if galaxies in any of the luminosity bins studied here are dominated by AGNs. In Fig.6, the ratios of two famous ULIRG Arp 220 (29.5) and Mrk 231 (5.9), the former a prototype of ‘cold ULIRGs’ which are mostly starbursts and the latter a prototype of ‘warm ULIRGs’ mostly AGNs, are also plotted as references. In addition to the intrinsic variations in the L_{dust}/L_{15} ratio, the effect of possible SED evolution in $z=0.6$ galaxies has to be taken into account, too.

The most direct way to constrain this uncertainty is to look at the real SEDs of the $z=0.6$ galaxies detected in longer wavelength bands of Spitzer, in particular the MIPS $160\mu m$ (rest-frame $100\mu m$) band. However, it turned out that only 1 source in the $z=0.6$ IR sample is detected at $160\mu m$ above the nominal 5σ sensitivity limit of $f_{160} = 100$ mJy (Surace et al. 2004). A much more robust method is to stack the $70\mu m$ and $160\mu m$ images of the galaxies in a given luminosity bin and use the mean f_{70}/f_{24} and f_{160}/f_{24} derived from the stacked images to constrain the mean SED. The $70\mu m$ and $160\mu m$ images are taken from the same SWIRE database. For each luminosity bin, SEDs taken from the sample plotted in Fig.6 are selected according to the IR luminosity range, the mean f_{70}/f_{24} and f_{160}/f_{24} and their uncertainties (including 20% calibration uncertainty). The mean L_{dust}/L_{15} ratio and the uncertainty are derived using these SEDs. The results are given in Table 3 and Table 4, and plotted in Fig.7. Note that for UV galaxies in the luminosity bin of $9.6 \leq \log(L_{FUV}/L_{\odot}) < 9.9$, no detections are found even on the stacked $70\mu m$ and $160\mu m$ images, therefore only upperlimits are listed. For galaxies in other luminosity bins in both Table 3 and Table 4, the detections on stacked

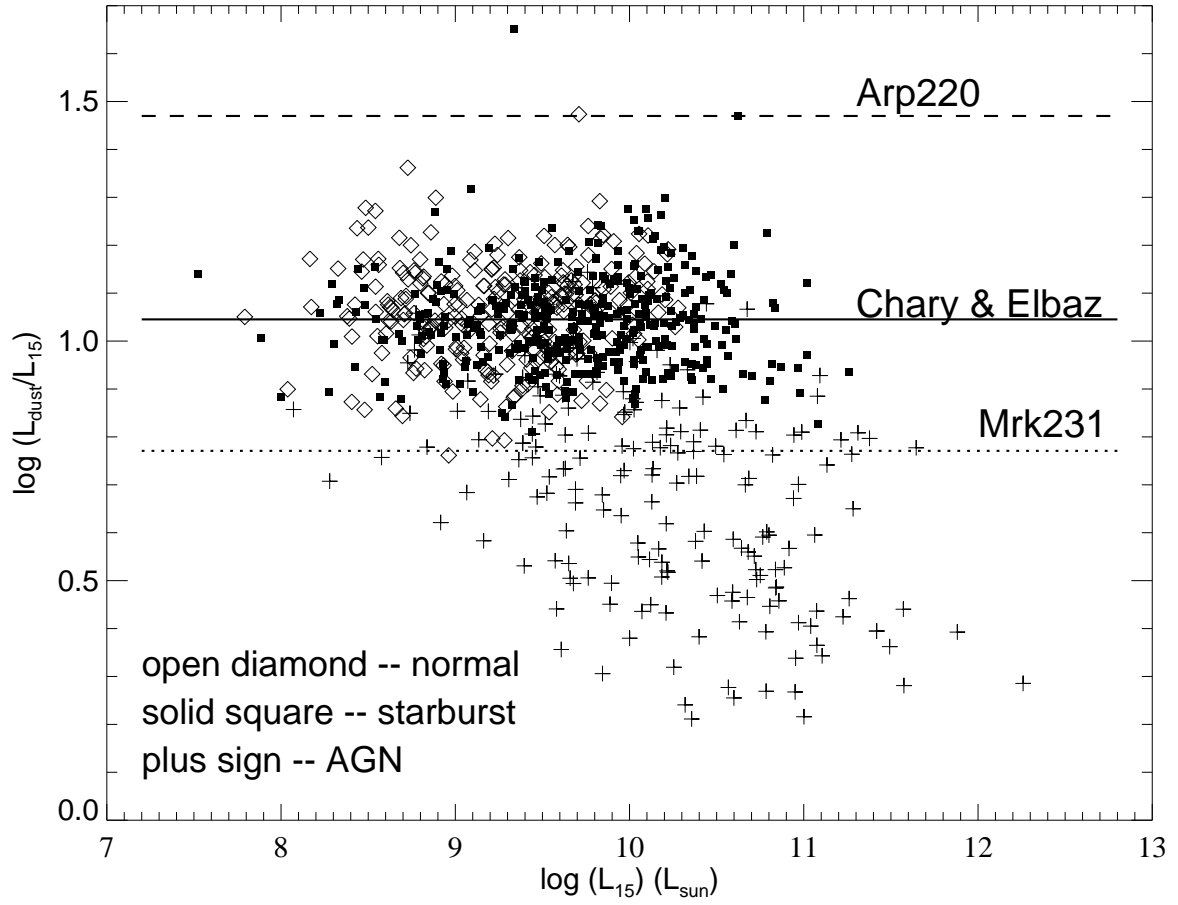


Fig. 6.— L_{dust}/L_{15} v.s. L_{15} plot for local IR galaxies in the SED library of Xu et al. (2001).

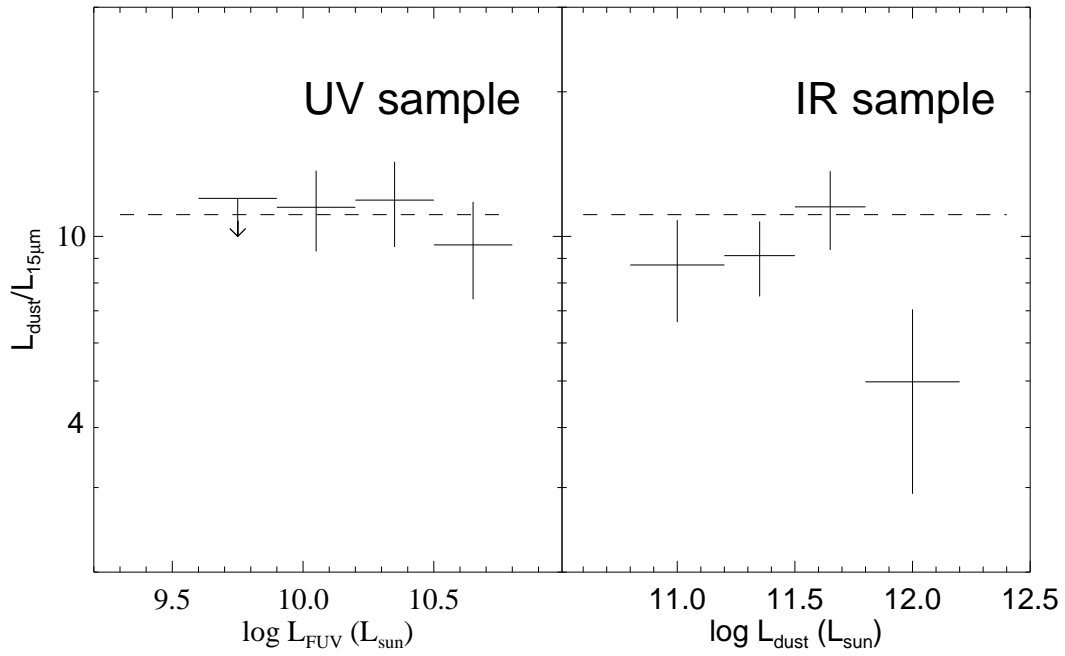


Fig. 7.— Mean L_{dust}/L_{15} ratios for $z=0.6$ UV galaxies (left panel) and for $z=0.6$ IR galaxies (right panel), estimated using the mean f_{160}/f_{24} and f_{70}/f_{24} ratios derived by stacking. The dotted line specifies the adopted standard taken from Chary & Elbaz (2001).

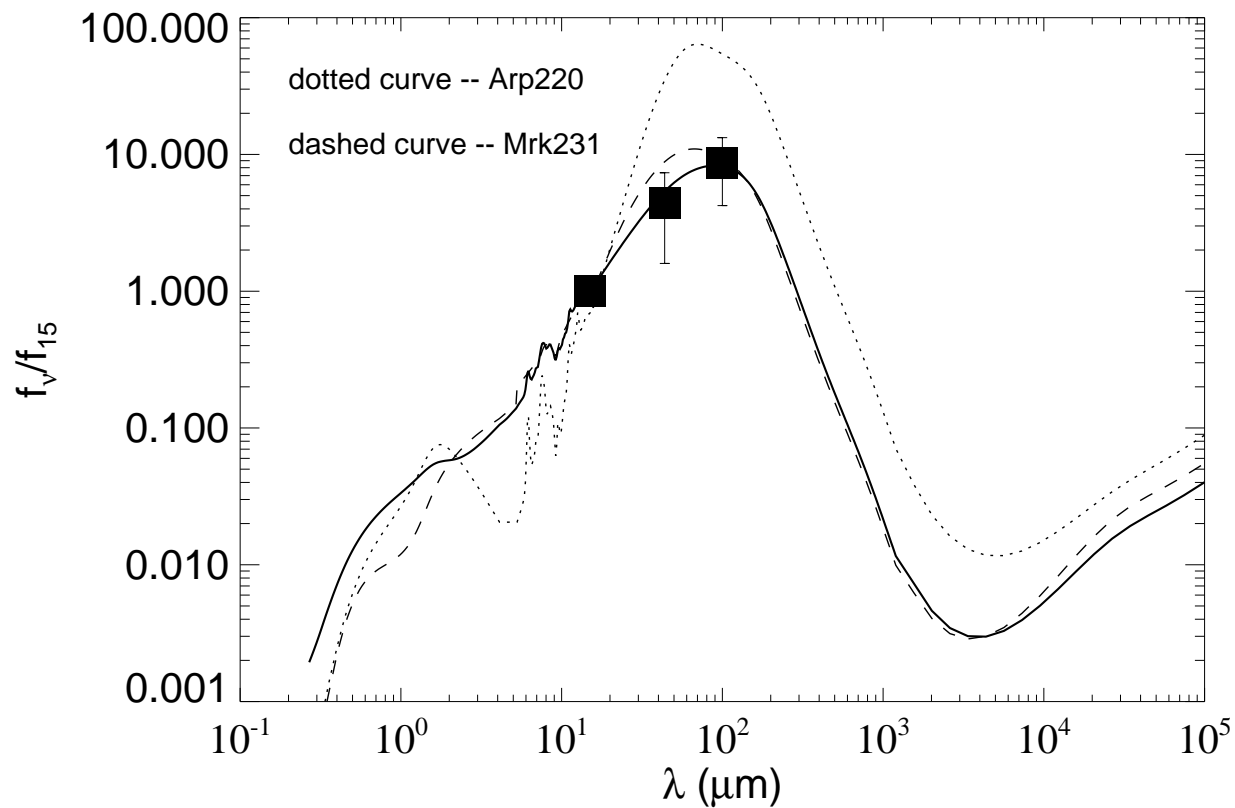


Fig. 8.— Plot of the rest-frame SED (solid curve) that fits the mean FIR color ratios (solid squares with error bars) of $z=0.6$ ULIRGs (IR galaxies of $11.8 \leq \log(L_{\text{dust}}/L_\odot) < 12.2$). Compared to the SED of Arp 220 (dotted curve) and that of Mrk 231 (dashed curve).

$70\mu m$ and $160\mu m$ images are significant (> 3 times of the noise), although some of the errors of the mean flux ratios (particularly those of f_{160}/f_{24}) are as high as 90%. In these cases the error of the mean is largely due to the statistical dispersion of the variable.

For all UV selected galaxies, the derived mean L_{dust}/L_{15} ratios for all the 4 luminosity bins are consistent with that of Chary and Elbaz (2001). For IR selected galaxies, only the mean ratio of galaxies in the brightest bin of $11.8 \leq \log L_{dust} < 12.2$ is significantly below the calibration of Chary and Elbaz (2001). As shown in Fig.8, the SED which fits the mean FIR colors of the bin is much closer to that of Mrk 231 than Arp 220, suggesting that many galaxies in this bin have their $24\mu m$ flux enhanced by AGN dust torus emission. This can be compared with the ISO results (Genzel et al. 1998) which show that most of the IRAS $60\mu m$ band selected $z=0$ ULIRGs of $L_{dust} \sim 10^{12}L_{\odot}$ are powered by starbursts, and AGN contribution is important only for ULIRGs with $L_{dust} > 2 \cdot 10^{12}L_{\odot}$ (Veilleux et al. 1998). The increased contribution in the MIR of AGN in the ULIRGs of our $z=0.6$ IR sample is at least partly a consequence of the MIR (rest-frame $15\mu m$) selection. Whether this also indicates a difference between $z=0$ and $z=0.6$ ULIRGs requires further investigation. Meanwhile, as shown in Fig.3, if the mean L_{dust} of the $z=0.6$ galaxies in the last luminosity bin is reduced by a factor of 2, their L_{dust}/L_{FUV} ratio is still consistent with that of the local ULIRGs.

4.2. Source Confusion

The angular resolutions of the MIPS $24\mu m$ maps and GALEX NUV maps are very well matched, both having $FWHM \sim 6''$. The astrometry of GALEX sources is accurate to $\sim 1''$ (Seibert et al. 2005), and that of SWIRE sources is even better (Surace et al. 2004). This ensures minimal mismatches between sources in the two bands. The contamination from nearby foreground bright sources is insignificant in the measurement of the $24\mu m$ fluxes

Table 3. Mean FIR colors and L_{dust}/L_{15} ratios of $z=0.6$ UV galaxies.

| L_{FUV} (L_{\odot}) | f_{70}/f_{24} | <i>error</i> | f_{160}/f_{24} | <i>error</i> | L_{dust}/L_{15} | <i>error</i> |
|------------------------------|-----------------|--------------|------------------|--------------|-------------------|--------------|
| 9.75 ± 0.15 | < 11.4 | ... | < 24.4 | ... | < 12.0 | ... |
| 10.05 ± 0.15 | 6.1 | 3.0 | 27.8 | 20.2 | 11.5 | 2.2 |
| 10.35 ± 0.15 | 10.3 | 4.7 | 38.9 | 25.0 | 11.9 | 2.4 |
| 10.65 ± 0.15 | 4.1 | 3.0 | 19.3 | 14.2 | 9.6 | 2.2 |

of the NUV sources. According to published $24\mu\text{m}$ number counts (Papovich et al. 2004; Shupe et al. 2006), the chance for a random source of $f_{24} > 0.2$ mJy to fall into the beam of an NUV source is less than 1%. For the measurement of the NUV fluxes of $24\mu\text{m}$ sources, the chance of this contamination is higher (at $\sim 2\%$ level according to the NUV counts of Xu et al. 2005). In order to minimize it, we did the stacking of the NUV images after subtracting sources brighter than $\text{NUV}=23.5$ mag (Section 3.1). Our choice of using the ‘trimmed mean’ to estimate the average fluxes in the luminosity bins should exclude sources seriously affected by bright neighbors. The confusion due to fainter sources adds another noise (confusion noise) to the total error budget. It could biases the measured flux of a stacked image to higher value only if the source population is strongly clustered (Takeuchi & Ishii 2004). For the NUV and $24\mu\text{m}$ sources, this is not the case. Heinis et al. (2004) found that UV galaxies are only very weakly clustered. For the $24\mu\text{m}$ sources, as shown by Zheng et al. (2006), the confusion noise behaves very close to the random Gaussian noise down to very faint flux level ($\sim 0.3\text{--}0.4\mu\text{Jy}$). Uncorrelated confused sources add an uniform diffuse background on the image, which is subtracted in the normal background subtraction task during the flux measurement. In summary, uncertainties due to source confusion are unlikely to introduce significant bias to our results.

5. Discussion

5.1. Difference between $z=0.6$ and $z=0$ LIRGs

In their study of faint galaxies in GOODS-N field, Melbourne et al. (2005) concluded that there is strong evidence for a morphological evolution of the populations of LIRGs since redshift $z=1$. They found that above $z=0.5$, roughly half of all LIRGs are spirals and the peculiar/irregular-to-spiral ratio is ~ 0.7 , whereas at low z , spirals count for only one-third of

Table 4. Mean FIR colors and L_{dust}/L_{15} ratios of $z=0.6$ IR galaxies.

| L_{FUV} (L_{\odot}) | f_{70}/f_{24} | <i>error</i> | f_{160}/f_{24} | <i>error</i> | L_{dust}/L_{15} | <i>error</i> |
|------------------------------|-----------------|--------------|------------------|--------------|--------------------------|--------------|
| 11.0 ± 0.2 | 3.9 | 2.0 | 15.0 | 13.8 | 8.7 | 2.1 |
| 11.35 ± 0.15 | 4.7 | 1.5 | 21.2 | 8.4 | 9.1 | 1.6 |
| 11.65 ± 0.15 | 6.5 | 1.8 | 31.7 | 13.2 | 11.5 | 2.2 |
| 12.0 ± 0.2 | 4.4 | 2.3 | 8.5 | 8.1 | 5.0 | 2.1 |

LIRGs and the peculiar/irregular-to-spiral ratio is 1.3. Similarly, Bell et al. (2005) found that at $z \sim 0.7$, the IR luminosity density for $10.7 \lesssim \log(L_{\text{IR}}/L_{\odot}) \lesssim 11.5$ is dominated by spiral galaxies, and the contribution from clearly interacting galaxies with morphology suggestive of major mergers is at most 30%. Our result of the significantly lower mean $L_{\text{dust}}/L_{\text{FUV}}$ ratios (i.e. dust attenuation) for the $z=0.6$ LIRGs compared to those of their local counterparts, is in line with these findings. As shown in local samples (Sanders & Mirabel 1996), non-interacting LIRGs usually are large, gas-rich spirals with widely distributed star formation all over the disk. In contrast, most of major-merger LIRGs have their starformation concentrates in the nuclei. These nuclear starbursts are highly compact, and they generally show very high dust attenuation (and warmer IR colors). If indeed the composite of LIRGs has changed from spiral dominant at $z \sim 0.6$ to major-merger dominant at $z=0$, the increase of the mean dust attenuation for these galaxies since $z=0.6$, as revealed in this work, is expected. On the other hand, even at high z , the population of ULIRGs is still dominated by major-mergers (Bell et al. 2005). This provides a simple explanation on why the difference between the mean $L_{\text{dust}}/L_{\text{FUV}}$ ratios of $z=0.6$ and $z=0$ galaxies does not extend to higher luminosity bins in Fig.3.

5.2. Evolution of cosmic dust attenuation

There has been strong evidence for a positive (backward) evolution of the mean dust attenuation in star forming galaxies of $z \lesssim 1$ (Takeuchi et al. 2005b). From the GALEX deep survey of VVDS field, Schiminovich et al. (2005) derived an evolution rate for the UV luminosity density up to $z=1$ in the form of $\rho_{1500\text{\AA}} \propto (1+z)^{2.5 \pm 0.7}$; at the same time, Le Floch et al. (2005) found from the Spitzer MIPS $24\mu\text{m}$ deep survey of the CDFS field that the IR luminosity function evolves between $0 \leq z \leq 1$ as $L_{\text{IR}}^* \propto (1+z)^{3.2^{+0.7}_{-0.2}}$ and $\phi_{\text{IR}}^* \propto (1+z)^{0.7^{+0.2}_{-0.6}}$, corresponding to an IR luminosity density evolution of $\rho_{\text{IR}} \propto (1+z)^{3.9}$. Therefore, the ratio between the IR and UV luminosity densities increases by a factor of $(1+0.6)^{1.4} = 1.9$ from $z=0$ to $z=0.6$, indicating a significant increase of cosmic dust attenuation during this redshift interval.

Interestingly, in this work, it is found that for galaxies of given UV or IR luminosities the dust attenuation did not increase with the redshift. Actually, there is evidence that the dust attenuation in $z=0.6$ LIRGs is even *lower* than that in the local LIRGs. Is this consistent with the positive backward evolution of cosmic dust attenuation? The key to understanding the apparent contradiction lies in the strong dependence of the dust attenuation on the SFR (Buat & Burgarella 1998; Heckman et al. 1998; Martin et al. 2005; Xu et al. 2006), and in the fact that SFR of the ‘average’ starforming galaxy at $z=0.6$ is much higher than the

‘average’ starforming galaxy at $z=0$. It is worthwhile to check out whether this interpretation works quantitatively. Assume the SFR of the average starforming galaxy evolving as $(1+z)^3$, which is consistent with luminosity evolution of both UV and IR galaxies. Then take the local ($z=0$) $L_{\text{dust}}/L_{\text{FUV}}$ versus SFR relation, which can be approximated by a linear dependence $L_{\text{dust}}/L_{\text{FUV}} \propto \text{SFR}$ above $\text{SFR} \sim 0.1 M_{\odot} \text{ yr}^{-1}$ (Xu et al. 2006). Accordingly, from $z=0$ to $z=0.6$, the average $L_{\text{dust}}/L_{\text{FUV}}$ ratio should increase by a factor of $(1+0.6)^3 = 4.1$, about a factor of 2 more than what is observed. Hence, it appears that combining the cosmic SFR evolution with local $L_{\text{dust}}/L_{\text{FUV}}$ versus SFR relation predicts *too much* evolution of cosmic dust attenuation. This again suggests that the major population of starforming galaxies at $z=0.6$, of which contribution from LIRGs can be significant (Hammer et al. 2005; Bell et al. 2005), may have less dust attenuation than that of $z=0$ galaxies of the same SFR.

6. Conclusion

Using new SWIRE observations in the IR and GALEX observations in the UV, we study the dust attenuation and stellar mass of two samples of $z \sim 0.6$ galaxies in the SWIRE/GALEX field ELAIS-N1-00 ($\Omega = 0.8 \text{ deg}^2$). The first sample is UV selected, having 600 galaxies with photometric redshift $0.5 \leq z \leq 0.7$ and $\text{NUV} \leq 23.5 \text{ mag}$ (corresponding to $L_{\text{FUV}} \geq 10^{9.6} L_{\odot}$ for $z=0.6$). The second sample is IR selected, containing 430 galaxies with $f_{24\mu\text{m}} \geq 0.2 \text{ mJy}$ ($L_{\text{dust}} \geq 10^{10.8} L_{\odot}$ at $z=0.6$) and in the same photometric redshift range. The L_{dust} is derived from the rest-frame 15μ luminosity. The dust attenuation is estimated using the luminosity ratio $L_{\text{dust}}/L_{\text{FUV}}$. Because of the low $24\mu\text{m}$ detection rate (20%) of the UV galaxies and the low UV detection rate (27%) of the IR galaxies, the stacking technique is exploited in deriving mean $L_{\text{dust}}/L_{\text{FUV}}$ ratios in given L_{FUV} and L_{dust} bins for UV and IR selected samples, respectively. The stellar mass is derived using the SWIRE $3.6\mu\text{m}$ flux which measures the rest-frame K-band $2.2\mu\text{m}$ emission. These results are compared to $L_{\text{dust}}/L_{\text{FUV}}$ ratios and the stellar mass of galaxies in control samples at $z=0$. It is found that the mean $L_{\text{dust}}/L_{\text{FUV}}$ ratios of the $z=0.6$ UV galaxies are consistent with that of their $z=0$ counterparts of the same L_{FUV} . For IR galaxies, the mean $L_{\text{dust}}/L_{\text{FUV}}$ ratios of the $z=0.6$ LIRGs are about a factor of 2 lower than local LIRGs, whereas $z=0.6$ ULIRGs have the same mean $L_{\text{dust}}/L_{\text{FUV}}$ ratios as their local counterparts. This is consistent with results in the literature that show evidence of population changes of LIRGs from major-merger dominant at $z=0$ to spiral dominant at $z > 0.5$. The stellar mass of $z=0.6$ UV galaxies of $L_{\text{FUV}} \leq 10^{10.2} L_{\odot}$ is about a factor 2 less than their local counterparts of the same luminosity, indicating growth of these galaxies. The mass of $z=0.6$ UVLGs ($L_{\text{FUV}} > 10^{10.2} L_{\odot}$) and IR selected galaxies, which are nearly exclusively LIRGs and ULIRGs, is the same as their local counterparts.

Acknowledgments:

GALEX (Galaxy Evolution Explorer) is a NASA Small Explorer, launched in April 2003. We gratefully acknowledge NASA's support for construction, operation, and science analysis for the GALEX mission, developed in cooperation with the Centre National d'Etudes Spatiales of France and the Korean Ministry of Science and Technology. Support for this work, part of the Spitzer Space Telescope Legacy Science Program, was provided by NASA through an award issued by JPL under NASA contract 1407. This publication makes use of data products from the Two Micron All Sky Survey, which is a joint project of the University of Massachusetts and the Infrared Processing and Analysis Center/California Institute of Technology, funded by NASA and NSF.

REFERENCES

- Arnouts, S., Schiminovich, D., Ilbert, O., Tresse, L., et al. 2005, ApJL, 619, 43.
- Bell, E.F., McIntosh, D.H., Katz, N., Weinberg, M.D., 2003, ApJS, 149, 289.
- Bell, E.F. Papovich, C., Wolf, C. Le Floch, E. et al. 2005, ApJ, 265, 23.
- Babbedge, T., et al. 2006, MNRAS, 370, 1159.
- Babbedge, T., et al. 2004, MNRAS, 353, 654.
- Blain, A.W., Smail, I., Ivison, R.J., Kneib, J.-P. 1999, MNRAS, 302, 632.
- Budavari, T., et al. 2005, ApJL, 619, 31.
- Buat, V., Burgarella, D. 1998, A&A, 334, 772.
- Buat, V., Xu, C. 1996, A&A, 306, 61.
- Buat, V., et al. 2005, ApJL, 619, 51.
- Buat, V., et al. 2006, this volume.
- Burgarella, D., Pérez-González, P.G., Tyler, K.D., et al., 2006, A&A, 450, 69.
- Burgarella, D., Buat, V., Iglesias-Páramo, J 2005, MNRAS, 360, 1413
- Chary, R.R., Elbaz, D. 2001, ApJ, 556, 562.
- Cole, S., Norberg, P., Baugh, C.M., et al. 2001, MNRAS, 326, 255.
- Combes, F., in *Proceedings of IAU Symp 235, "Galaxy Evolution across the Hubble Time"*,
Eds. F. Combes & Jan Palous, Cambridge Univ Press, preprint (astro-ph/0608612).
- Fazio, G.G., et al. 2004, ApJS, 154, 39.
- Flores, H., Hammer, F., Desért, F.X., Césarsky, C., et al. 1999a, A&A, 343, 389.

- Franceschini, A., Aussel, H., Cesarsky, C.J., Elbaz, D., Fadda, D., 2001, *A&A*, 378, 1.
- Franceschini, A., et al. 2005, *AJ*, 129, 2074.
- Genzel, R., Lutz, D., Sturm, E., Egami, E., et al. 1998, *ApJ*, 498, 579.
- Gordon, K., Clayton, G.C., Witt, A.N., Misselt, K.A. 2000, *ApJ*, 533, 236.
- Hatziminaoglou, E., Prez-Fournon, I., Polletta, M., Afonso-Luis, A., et al. 2005, *AJ* 129, 1198.
- Hammer, F., Flores, H., Elbaz, D. et al, 2005, *A&A*, 430, 115.
- Heavens, A., Benjamin, P., Jimenez, R. Dunlop, J. 2004, *Nature*, 428, 625.
- Heckman, T.M., Hoopes, C.G., Seibert, M., Martin, D.C., et al. 2005, *ApJL*, 619, 35.
- Heckman, T.M., Robert, C.; Leitherer, C., Garnett, D.R., van der Rydt, F. 1998, *ApJ*, 503, 646.
- Heinis, S., Treyer, M., Arnouts, S., Milliard, B., et al. 2004, *A&A Lett*, 424, 9.
- Houck, J.R., Soifer, B.T., Weedman, D., Higdon, S.J.U., et al. 2005, *ApJL*, 622, 105.
Garnett, D.R., van der Rydt, F. 1998, *ApJ*, 503, 646.
- Iglesias-Páramo, J. Buat, V., Donas, J., Boselli, A., Milliard, B. 2004, *A&A*, 419, 109.
- Iglesias-Páramo, J. et al. 2006, *ApJS*, 164, 38.
- Jarrett, T., Chester, T., Cutri, R., et al. 2000, *AJ*, 119, 2498.
- Kroupa, P., Tout, C.A., Gilmore, G. 1993, *MNRAS*, 262, 545.
- Lilly, S.J., Le Fèvre, O., Hammer, F., Crampton, D. 1996, *ApJ*, 460, L1.
- Le Floch, E. Papovich, C., Dole, H. et al. 2005, *ApJ*, 632, 169.
- Lonsdale, C., et al. 2004, *ApJS*, 154, 54. 2005, *ApJ*, 632, 169.
- Madau, P., Ferguson, H.C., Dickinson, M., Giavalisco, M., et al. 1996, *MNRAS*, 283, 1388.
- Martin, D.C., et al., 2005, *ApJL*, 619, 59.
- Meurer, G.R., Heckman, T.M., Calzetti, D. 1999, *ApJ*, 521, 64.
- Melbourne, J., Koo, D.C., Le Floch, E. 2005, *ApJL*, 632, 65.
- Papovich, C., Dole, H., Egami, E., Le Floch, E., et al. 2004, *ApJS*, 154, 70.
- Pérez-Fournon, I., et al. 2006: in preparation.
- Rowan-Robinson, M. 2003, *MNRAS*, 345, 819.
- Rowan-Robinson, M., Babbedge, T., Surace, J., Shupe, D., et al. 2005, *AJ*, 129, 1183.
- Sanders, D.B. & Mirabel, I.F. 1996, *ARAA*, 34, 749.

- Saunders, W., Sutherland, W.J., Maddox, S.J., et al. 2000, MNRAS, 317, 558.
- Schiminovich, D., Ilbert, O., Arnouts, S., Milliard, B., et al. 2005, ApJL, 619, 47.
- Schlegel, D.J., Finkbeiner, D.P., Davis, M. 1998, ApJ, 500, 525.
- Seibert, M. et al., 2005, ApJL, 619, 23.
- Serjeant, S., et al. 2006, in preparation.
- Shupe, D.L., et al., 2006, submitted to AJ.
- Surace, J.A., Sanders, D.B., Evans, A.S. 2000, ApJ, 529, 170.
- Surace, J.A., Shupe, D.L., Fang, F., Lonsdale, C. J., et al., 2004, Cat., 2255; "SWIRE ELAIS N1 Source Catalogs".
- Takeuchi, T.T., Buat, V., Iglesias-Páramo, J., Burgarella, D. 2005a, A&A, 432, 423.
- Takeuchi, T.T., Buat, V., Burgarella, D. 2005b, A&A, 440, L17.
- Takeuchi, T. T., Ishii, T. T. 2004, ApJ, 604, 40.
- Veilleux, S., Sanders, D.B., Kim, D.-C. 1998, ApJ, 522, 139.
- Wang, B., Heckman, T.M. 1996, ApJ, 457, 645.
- Xu, C., 2000, ApJ, 541, 134.
- Xu, C., Buat, V. 1995, A&A Letters, 293, 65.
- Xu C.K., Buat, V., Iglesias-Páramo, J., Takeuchi, T.T., et al., 2006, ApJ, 646, 834.
- Xu C.K., Donas, J., Arnouts, S., Wyder, T.K., et al. 2005, ApJL, 619, 11.
- Xu, C., Lonsdale, C.J., Shupe, D.L., O'Linger, J., Masci, F. 2001, ApJ, 562, 179.
- Yan, L., Chary, R., Armus, L., et al. 2005, ApJ, 628, 604.
- Zheng, X.Z., Bell, E.F., Rix, H.-W., Papovich, C., et al. 2006, ApJ, 640, 784.